Available on: http://gjetr.ep-journals.org/ E-ISSN: 3051-3782, P-ISSN: 3051-3774

Global Journal of Engineering and Technology Review

Volume: 01 Issue: 04 December 2025

Swing Bus Placement Location's Impact on the Distance Buses in an Electric Grid Network (Case Study of Nigeria Transmission 330kv Lines Network)

Asuquo Eke
Department of Electrical/Electronic Engineering, University of Cross River State, Calabar, Nigeria

Ake David
Department of Electrical/Electronic Engineering, Admiralty University of Nigeria, Delta State, Nigeria

E.J. Akpama
Department of Electrical/Electronic Engineering, University of Calabar, Cross River State, Nigeria

O. I. Okoro
Department of Electrical/Electronic Engineering, Michael Okpara University of Agriculture, Umudike, Abia state, Nigeria

Published Date: December 05, 2025 **Article DOI:10.65150/EP-gjetr/V1E4/2025-03**

ABSTRACT: Using Nigeria's 330kV transmission lines network as a case study, this paper examines how swing bus placement site affects the spacing between buses in an electric grid network. In power system analysis, especially load flow studies, the swing bus is essential. The accuracy and convergence of load flow solutions can be strongly impacted by the swing bus's location. The impact of various swing bus placements on the spacing between buses in the Nigerian 330kV transmission network is examined in this research using ETAP. The findings indicate that the swing bus's location has an impact on the network's power flow, line losses, and voltage profile. Decisions on power system design and operation can be influenced by the study's insights regarding the swing bus's ideal location inside the Nigerian grid network. The results show that, toward the northern part of the network, due to the long distance, the system violate the voltage limits in almost all the busses. The system frequency limit also affected. Since the swing bus sets a reference voltage angle, its location affects system-wide voltage phase angles. A choice distorts the voltage profile, especially in radial, weakly meshed sections area of the network. Swing bus position affects how losses are circulated and distributed across the lines. Most buses' voltage angles exhibit a noticeable drop from 0.02 seconds to about 2-3 seconds, after which they either stabilize or barely fluctuate. This can suggest a response to a problem or disturbance. The voltage levels begin to climb again by 7.5 to 15 seconds after first decreasing (especially between 1 and 5 seconds), indicating that the system has stabilized.

KEYWORDS: Swing Bus Placement, Electric Grid Network, Load Flow Analysis, Transmission Line Stability, Nigeria 330kV Network

1. INTRODUCTION

The placement of swing buses, and long-distance electric buses within the same electrical network provides considerable environmental advantages and potential long-term cost reductions. Nonetheless, it presents notable challenges related to load management, infrastructure investment, and technical coordination. Successful management of these impacts on the electrical network requires effective planning, investment in smart charging infrastructure, and the use of renewable energy sources. [] Introducing a fleet of electric buses, including both swing and long-distance types, will substantially elevate the demand on the electricity network. Long-distance buses, which have larger batteries, will contribute significantly more load compared to those on shorter routes. Charging schedules must be meticulously managed to prevent peaks in demand, particularly during periods when the electricity network is already stressed. Implementing coordinated charging strategies, such as off-peak charging, can help alleviate this issue. Adequate charging infrastructure is essential for both swing and long-distance buses. Long-distance buses, in particular, may require high-power fast chargers, necessitating substantial investments in electrical infrastructure. Enhancing the electricity network's capacity may be necessary to accommodate the increased load. This could involve reinforcing substations, distribution lines, and potentially transmission infrastructure. Deploying energy storage systems, such as battery storage, can help balance the load by storing energy during low-demand periods and supplying it during peak-demand times. To enhance environmental benefits, the electricity used for charging buses should be sourced from renewable energy. This necessitates a strong integration of renewable resources like solar and wind into the grid. Promoting distributed generation, such as installing solar panels at bus depots, can decrease the load on the central grid and provide local power for charging. Upfront capital expenditures for infrastructure related to charging and possible grid improvements are substantial. These expenses must be weighed against the long-term savings from lower maintenance and fuel expenditures. The bus fleet's operating expenses will be impacted by the price of power, both peak and off-peak rates. Cost-effective energy management techniques can aid in maximizing these expenses. Rewards and Subsidies Incentives

License: This is an open access article under the CC BY 4.0 license: https://creativecommons.org/licenses/by/4.0/

from the government for the installation of electric vehicle (EV) infrastructure can help reduce costs. Policies that encourage the use of EVs and renewable energy are essential. Upfront investments are high for infrastructure related to charging and possible grid improvements. The long-term benefits from lower maintenance and fuel expenses must be weighed against these expenses. Operational Costs: The cost of power, both peak and off-peak rates, will affect the fleet's operating expenses. These costs can be optimized with the use of efficient energy management techniques. Promotions and Grants: Some of the cost pressures can be reduced by government subsidies for electric vehicle (EV) infrastructure. Policies must encourage the use of EVs and renewable energy. When driven by renewable energy, electric buses significantly lower greenhouse gas emissions and local air pollution. Bus routes and metropolitan areas are less noisy when it comes to noise pollution since electric buses are quieter than diesel buses. By switching to electric buses, the public's opinion of public transportation may be enhanced, which could lead to an increase in ridership and support for environmentally friendly programs. It is difficult yet crucial to effectively plan the locations and times of charging for swing and long-distance buses. Smart charging systems can optimize charging schedules based on current grid conditions and bus schedules. Batteries need to be appropriate for swing and long-distance buses in terms of both range and recharge times. Developments in technology are required for the safety of the equipment. The integration will benefit from advancements in battery technology, such as increased energy densities and faster charging times. It's essential to have a dependable power source when charging. To prevent interruptions, redundancy measures like backup generators or extra grid connections could be required. Since swing buses run more frequently during the day than far-distance buses do, there may be more frequent but smaller spikes in the amount of electricity used at charging stations. Grid Stability: To ensure grid stability, the introduction of swing and long-distance buses necessitates strict control over electrical demand. This entails taking capacity limitations, and peak demand periods, and making sure the grid infrastructure is large enough to accommodate changing load profiles.

2. METHODOLOGY

(A) Modeling of Typical Transmission Network:

The typical transmission line is presented as a single-line diagram shown in Figure 3.1a

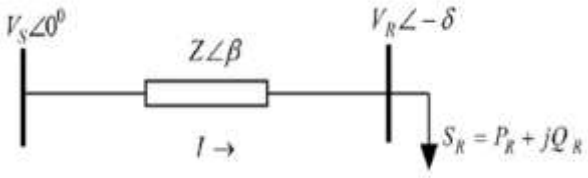


Figure 1.0: Single Line Diagram of Transmission Line

In the context of power system stability, managing reactive power and voltage is particularly crucial. The issue is preventing voltage instability, which might result in voltage collapse. Reactive power is crucial for maintaining a constant system voltage (Gupta and Sharma, 2013). It is created when the current waveform deviates from the voltage waveform due to energy-saving elements like capacitors or inductors. Reactive power is required to reduce the electric and magnetic fields in the capacitor and inductor, respectively. The voltage of the transmission line can be adjusted by varying the reactive power. This can be demonstrated.
as follows:

$$S_R = P_R + jQ_R \quad (1)$$

Therefore, equation (1) may be expressed as,

$$S_R = V_R\left\{\frac{V_S\cos\delta + JV_S\sin\delta - V_R}{JX}\right\} \quad (2)$$

$$S_R = \frac{V_R V_S\sin\delta}{X} + J\frac{V_R V_S\cos\delta - V_R^2}{X} \quad (3)$$

According to equation (3), the active and reactive power supplied to the load is:

$$P_R = \frac{V_R V_S\sin\delta}{X} \quad (4)$$

$$Q_R = \frac{V_R V_S\cos\delta - V_R^2}{X} \quad (5)$$

From equation (4) and (5), using $\sin^2\theta + \cos^2\theta = 1$, we have

$$P_R^2 + (Q_R + \frac{V_R^2}{X})^2 = \frac{V_S^2 V_R^2}{X^2} \quad (6)$$

The voltage at the receiving bus (bus-2) can be expressed as,

$$V_R^2 = \frac{1}{2}\left[V_S^2 - 2Q_R Z + V_S\left(\sqrt{V_S^2 - \frac{4P_R^2 Z^2}{V_S^2} - 4Q_R}\right)\right] \quad (7)$$

Where;

V_S and V_R are bus voltages at the sending and receiving end respectively;

I is the line current;

X is the reactant;

δ is the generator's internal angle;

P_S and P_R are active and reactive powers supplied to the load.

License: This is an open access article under the CC BY 4.0 license: https://creativecommons.org/licenses/by/4.0/

B. Formulation of Power Flow Equation in Transmission Network:

Power flow describes the flow of both active and reactive power via power system networks. There are reciprocal effects between the bus voltage magnitude and the power flow phase angles. Power flow studies are designed to offer information on bus voltage magnitudes, bus voltage angles, and the active and reactive power flow across various branches, generators, and loads under steady-state circumstances. The information is essential for evaluating the system's performance. In the power system network, which is made up of nth-buses, the current Ii injected at the ith bus is expressed as

$$I_i = \sum_{k=1}^{n} Y_{ik} V_k; i = 1,2 \dots \dots . n \quad (8)$$

Where;

I_i =the current in ith bus;

V_k = the voltage at bus k;

Y_{ik} = the admittance between bus i and bus k.

The complex power injected by the source into ith bus is described as,

$$S_i = V_i I_i : i = 1,2 \dots \dots \dots \dots . n \quad (9)$$

$$S_i = P_i + jQ_i \quad (10)$$

Equations (9) and (10) are modified into two equations given as,

$$I_i = \frac{S_i^*}{V_i^*} \quad (11)$$

$$I_i = \frac{P_i - jQ_i}{V_i^*} \quad (12)$$

From equation (12),

$$P_i - jQ_i = V_i^* I_i \quad (13)$$

Substituting equation (8) we have,

$$P_i - jQ_i = V_i^* (\sum_{k=1}^{n} Y_{ik} V_k); i = 1,2 \dots \dots . . n \quad (14)$$

Separating equation (29) into imaginary and real components we have,

$$P_i = \mathrm{Re}(V_i^* (\sum_{k=1}^{n} Y_{ik} V_k)) \quad (15)$$

$$Q_i = -\mathrm{Im}(V_i^* (\sum_{k=1}^{n} Y_{ik} V_k)) \quad (16)$$

Where V_i, V_i^*, V_k and Y_{ik} are expressed in polar form as follows

$$V_i = |V_i| e^{j\delta_i};\ V_i^* = |V_i^*| e^{-j\delta_i};\ V_k = |V_k| e^{j\delta_k};\ Y_{ik} = |Y_{ik}| e^{j\theta_{ik}} \quad (17)$$

Substituting equation (17) into equations (15) and (16), we have

$$P_i = |V_i| \sum_{k=1}^{n} |Y_{ik}||V_k| \cos(\theta_{ik} + \delta_k - \delta_i) \quad (18)$$

$$Q_i = -|V_i| \sum_{k=1}^{n} |Y_{ik}||V_k| \sin(\theta_{ik} + \delta_k - \delta_i) \quad (19)$$

A total of 2n power equations are generated from the static power flow equations (18) and (19). Because of its precision, dependability, and quicker rate of convergence, the Newton Raphson technique is used to solve the non-linear equations. The expression for the Newton-Raphson power flow is;

$$\begin{bmatrix} \Delta P \\ \Delta Q \end{bmatrix} = \begin{bmatrix} J_1 & J_2 \\ J_3 & J_4 \end{bmatrix} \begin{bmatrix} \Delta\delta \\ \Delta V \end{bmatrix} \quad (20)$$

Where;

ΔP is the real power mismatch;

ΔQ is the reactive power mismatch;

$\Delta\delta$ is the bus voltage mismatch;

J_1, J_2, J_3 and J_4 are the elements of the Jacobian matrix which are obtained by partial differentiation of equations (18) and (19) concerning the static variables (δ, V). The off-diagonal and diagonal matrix of J_1, J_2, J_3 and J_4 are expressed as follows:

The off-diagonal and diagonal matrix of J_1:

$$\frac{\partial P_i}{\partial \delta_k} = V_i V_k Y_{ik} \sin(\theta_{ik} + \delta_i - \delta_k), k \neq i \quad (21)$$

$$\frac{\partial P_i}{\partial \delta_k} = -\sum_{\substack{k=1 \\ k=i}}^{n} V_i V_k Y_{ik} \sin(\theta_{ik} + \delta_i - \delta_k) \quad (22)$$

The off-diagonal and diagonal matrix of J_2:

$$\frac{\partial P_i}{\partial V_k} = V_i Y_{ik} \cos(\theta_{ik} + \delta_i - \delta_k), k \neq i \quad (23)$$

$$\frac{\partial P_i}{\partial V_k} = 2V_i Y_{ii} \cos\theta_{ii} + \sum_{\substack{k=1 \\ k=i}}^{n} V_k Y_{ik} \cos(\theta_{ik} + \delta_i - \delta_k) \quad (24)$$

The off-diagonal and diagonal matrix of J_3:

$$\frac{\partial Q_i}{\partial \delta_k} = -V_i V_k Y_{ik} \cos(\theta_{ik} + \delta_i - \delta_k), k \neq i \quad (25)$$

$$\frac{\partial P_i}{\partial \delta_i} = \sum_{\substack{k=1 \\ k=i}}^{n} V_i V_k Y_{ik} \cos(\theta_{ik} + \delta_i - \delta_k) \quad (26)$$

The off-diagonal and diagonal matrix of J_4

$$\frac{\partial Q_i}{\partial V_k} = V_i Y_{ik} \sin(\theta_{ik} + \delta_i - \delta_k), k \neq i \quad (27)$$

$$\frac{\partial Q_i}{\partial V_i} = 2V_i Y_{ii} \sin\theta_{ii} + \sum_{\substack{k=1 \\ k=i}}^{n} V_k Y_{ik} \sin(\theta_{ik} + \delta_i - \delta_k) \quad (28)$$

License: This is an open access article under the CC BY 4.0 license: https://creativecommons.org/licenses/by/4.0/

The real and reactive power mismatches at each iteration with new estimates of the bus voltage angles and voltage magnitude are expressed as follows:

$$\Delta P_i^r = P_i^s - P_i^r \quad (29)$$

$$\Delta Q_i^r = Q_i^s - Q_i^r \quad (30)$$

$$\delta_i^{r+1} = \delta_i^r - \Delta\delta_i^r \quad (31$$

$$V_i^{r+1} = V_i^r - \Delta V_i^r \quad (32)$$

Where,

r is the iteration count;

ΔP_i^r is the real power mismatch at r-iteration;

P_i^S is the special value of real power;

P_i^r is the calculated value of real power at r-iteration;

ΔQ_i^r is the reactive power mismatch at r iteration;

Q_i^s is the special value of reactive power;

Q_i^r is the calculated value of reactive power at r-iteration;

$\delta_i^{r+1} = \delta_i^r - \Delta\delta_i^r$; $V_i^{r+1} = V_i^r - \Delta V_i^r$

δ_i^{r+1} is the new estimate of bus angle at iteration r+1;

δ_i^r is the calculated value of the bus voltage angle at r-iteration;

$\Delta\delta_i^r$ is the bus voltage angle mismatch at r-iteration;

V_i^{r+1} is the new estimate of bus voltage at iteration r+1;

V_i^r is the calculated value of the bus voltage at r-iteration;

ΔV_i^r is the bus voltage mismatch at r-iteration.

The voltage and reactive power constraints at each bus i are expressed as follows:

$$V_{i(min)} \leq V_i \leq V_{i(max)} \quad (33)$$

$$Q_{i(min)} \leq Q_i \leq Q_{i(max)} \quad (34)$$

Where; The minimum and maximum voltage values at bus I are denoted by V_(i(min)) and V_(i(max)); the minimum and maximum reactive power provided at bus I are denoted by Q_(i(min)) and Q_(i(max)). The continuous power flow (CPF) method has frequently been used to determine the system's maximum loading point. Conventional power flow algorithms often suffer from convergence problems at operating locations near the stability limit [16]. The CPF analysis fixes this problem by automatically changing the loading parameter value so that the user may see the whole voltage profile. The main objective of using CPF is to determine the continuous power flow solution for a certain load change. The mechanism of continuous power flow is explained in Figure 2.

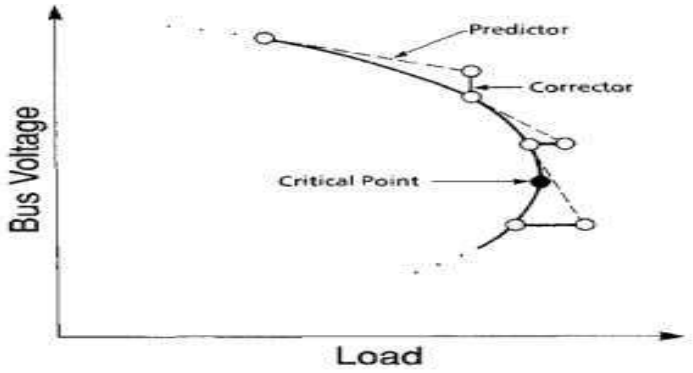


Figure 2: Continuation Power Flow method [10]

The concept of CPF is simple. It uses the predictor-corrector approach to solve a set of power flow equations that have been rebuilt with a load parameter. It starts with a known solution and predicts a subsequence solution that corresponds to a new value of the load parameter using a tangent predictor. The Newton-Raphson approach used for conventional power is then used to this estimate to make it more accurate. The formula for Continuation Power Flow Analysis is as follows [89]. P_{di} and Q_{di} can be expressed as follows when a load shift is simulated during the prediction phase

$$P_{di} = P_{di}^o(1 + \lambda * KP_{di}) \quad (36)$$

$$Q_{di} = Q_{di}^o(1 + \lambda * KQ_{di}) \quad (37)$$

The base case active and reactive power of the loads of phase P at bus I are denoted by P_di^o and Q_di^o, whereas the loading factor, λ, describes the load change. Likewise, the generator change P_giandQ_gi as a function of λ is represented as

$$P_{gi} = P_{gi}^o(1 + \lambda * KP_{gi}) \quad (38)$$

$$Q_{gi} = Q_{gi}^o(1 + \lambda * KQ_{gi}) \quad (39)$$

where λ is the loading factor and P_gi^o and Q_gi^o are the generator's base-case active and reactive power at bus I. To keep the PQ machine's power factor constant, the KP_gi/KQ_gi ratio remains constant. Eqn (39) is not necessary for a PV machine. Q_gi must be maintained at the limit when the reactive power limit is exceeded. An additional variable λ is added to the nonlinear power flow equations, which are expressed as

License: This is an open access article under the CC BY 4.0 license: https://creativecommons.org/licenses/by/4.0/

$$f(x,\lambda) = 0 \quad (40)$$

The estimated point for the solution is found using the prediction step. By taking a suitable size step in the direction tangent to the solution route, the next solution is predicted. The continuation method with predictor and corrector phases can be used to equation (40). When we linearize equation (40), we obtain

$$df(x,\lambda) = f_x dx + f_\lambda d\lambda = 0 \quad (41)$$

Equation (41), which requires a non-zero value for one of the tangent vectors and maintains its change at ± 1, is represented as

$$t_k = \pm 1 \quad (42)$$

where t_k represents the tangent vector dx's non-zero component. Equations (41) and (42) are combined to create a set of equations where the unknown variables dλ and dx are the tangent vectors. That's

$$\begin{bmatrix} f_x & f_\lambda \\ e_k & 0 \end{bmatrix}\begin{bmatrix} d_x \\ d_\lambda \end{bmatrix} = \begin{bmatrix} 0 \\ \pm 1 \end{bmatrix} \quad (43)$$

where e_k is a row vector where every other entry is equal to zero and kth is equal to 1. Either +1 or -1 can be used in equation (43) depending on how the kth state variable evolves during the trace of the solution. Equation (8) may be solved, and the expected next response is shown as

$$\begin{bmatrix} X^* \\ \lambda^* \end{bmatrix} = \begin{bmatrix} x \\ \lambda \end{bmatrix} + \sigma \begin{bmatrix} d_x \\ d_\lambda \end{bmatrix} \quad (44)$$

where σ is a scalar and * is the expected answer for the following step. The augmented Newton-Raphson power flow equation must be solved at the corrector stage, beginning with the anticipated solution of equation (44) as given by

$$\begin{bmatrix} f(x,\lambda) \\ x_k - \eta \end{bmatrix} = \begin{bmatrix} 0 \\ 0 \end{bmatrix} \quad (45)$$

Newton Raphson's method may be used to solve the corrector problem below, where j is the expected value of the continuation parameter x_k (Gupta and Sharma, 2013).

$$\begin{bmatrix} f_x & f_\lambda \\ e_k & 0 \end{bmatrix}\begin{bmatrix} \Delta_x \\ \Delta_\lambda \end{bmatrix} = \begin{bmatrix} f(x,\lambda) \\ x_k - \eta \end{bmatrix} \quad (46)$$

The operating limit of generators that are to satisfied are taken as:

$$I_a \le I_a^{max} \quad (47)$$

$$I_f^{min} \le I_f \le I_f^{max} \quad (48)$$

$$E_f^{min} \le E_f \le E_f^{max} \quad (49)$$

$$P_g^{min} \le P_g \le P_g^{max} \quad (50)$$

$$Q_g^{min}(P_g) \le P_g \le Q_g^{max}(P_g) \quad (51)$$

In this case, I_a^max represents the generator stator winding's current limit; I_f^min and I_f^max represent the generator rotor winding's minimum and maximum current limits, respectively; E_f^min and E_f^max represent the corresponding excitation voltage limit; P_g^min and P_g^max represent the minimum and maximum active power limits; and Q_g^min and Q_g^max represent the minimum and maximum reactive power limits, respectively.

3.0 RESULTS AND DISCUSSION

Table 1: Table of bus results showing the impacts of swing bus on the selected buses

Time (Sec)/ Bus Id.	0.020	1.00	1.5	2.0	2.5	3.0	5.0	7.5	10.0	12.5	15.0
Ikot Abasi V. ang	169.7	128.2	52.9	51.6	24.9	36.9	5.29	4.58	13.9	11.5	18.9
(Deg)	96.7%			96.7%	96.1	95.0	95.1%	99.2%	97.5%	99.1%	102%
Voltage (volt)	50.0	49.4	50.8	50.5	4895	47.38	43.2	47.47	484	49.1	49.99
Freq (Hz)											
Kaduna V. Ang	161.2	121.7	53.1	50.0	25.8	23.7	11.2	4.11	15.1	9.66	18.6
(Deg)	101.6%			102.3%			93.2%	94.1%	91.9%	94.2%	90.1%
Voltage (volts)	50.0	49.4	50.3	50.49	48.9	47.4	43.23	47.55	48.4	49.1	49.91
Freq(Hz)											
Owerri V. Ang	168.6	119.3	51.3	49.6	20.22	22.6	7.10	5.55	14.10	9.44	17.5
(Deg)	101.5%			103.4%			95.1%		95.1%	99.4%	98.9%
Voltage (volts)	50.0	49.45	50.03	50.5	49.47	47.3	43.31	47.5	48.4	49.1	50.0
Freq(Hz)											
Egbin V. Ang	0.0	0.0	0.0	0.0	0.0	0.0	0.0	0.0	0.0	0.0	0.0
(Deg)	100%			104.0%			98.8%	101.2%	98.2%	99.1%	102.1%
Voltage (volts)	50.0	51.9	52.0	51.8	50	49.2	48.0	50.0	51.1	51.3	51.9
Freq (Hz)											
Maduguri V.Ang	161.9	118.5	57.8	45.0	29.3	22.9	13.2	0.31	11.1	7.98	14.7
(Deg)	106.3%			105.6%	109.9%	112%	92.2%	90.3%	91.1%	109.1%	109.3%
Voltage(%volts)	50.0	49.41	52.0	51.9	48.98	47.43	42.2	47.3	48.9	49.8	49.99
Freq(Hz)											
Alagbon V. ang	168.9	113.4	51,7	47.5	18.8	15.14	8.8	4.92	12.6	7.6	15.56

License: This is an open access article under the CC BY 4.0 license: https://creativecommons.org/licenses/by/4.0/

Corresponding Author: Asuquo Eke

(deg)	99.5%			99.45%	95.4%	94.8%	98.2%	97.2%	95.5%	99.6%	103%
%Voltage(volts)	50.0	50.05	50.46	49.1	50.1	45.3	47.9	48.4	49.1	49.5	50.1
Freq(Hz)											

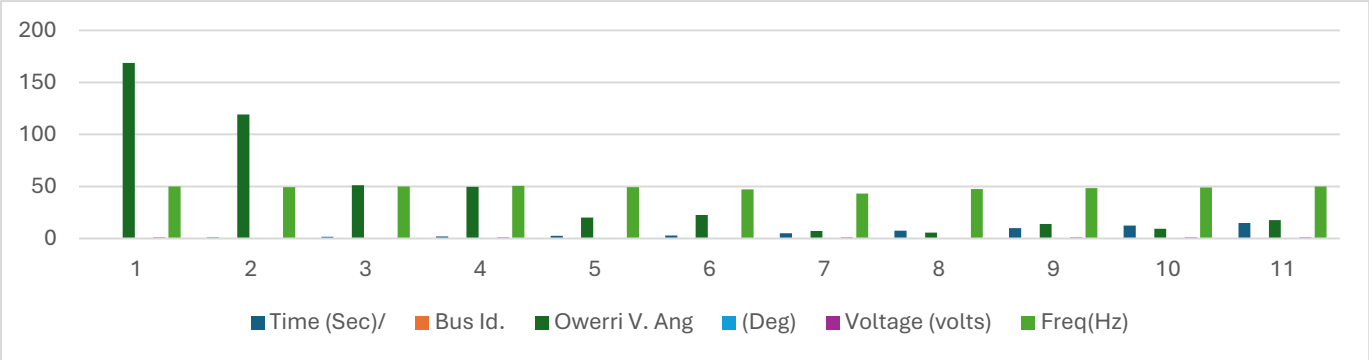


Fig.3: graph of Owere bus

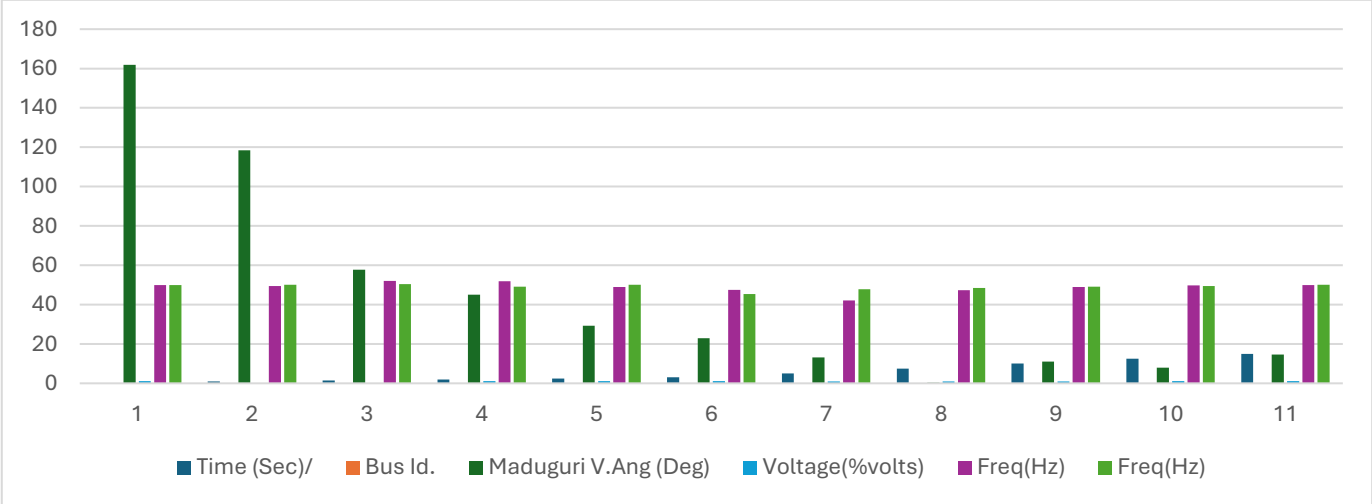


Fig.4: graph of Alagbon bus

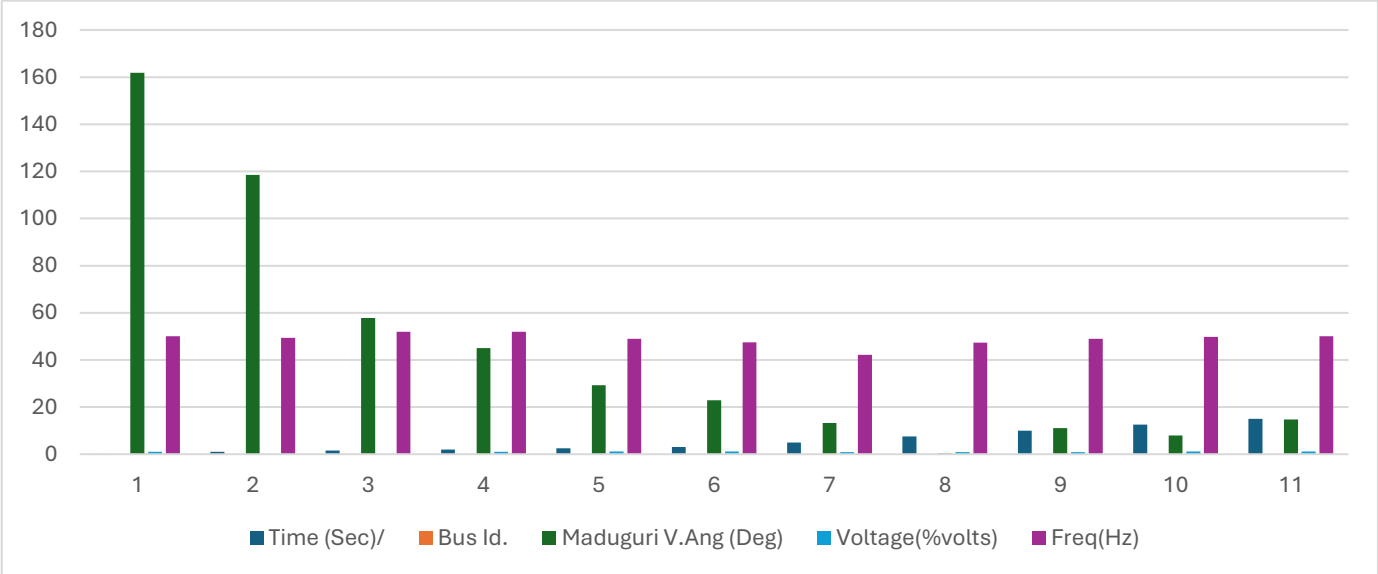


Fig.5: graph of Maduguri bus

In figure 3 and figure 4, the early spike in sudden load or disconnection, after spike, the values stabilize, and frequency remains steady, suggesting the system reaches a new stability. The voltage angle of the majority of buses shows a notable decrease from 0.02 seconds to around 2-3 seconds,

License: This is an open access article under the CC BY 4.0 license: https://creativecommons.org/licenses/by/4.0/

after which it either stabilizes or varies little. This could imply a reaction to an issue or disruption. After initially declining (particularly between 1 and 5 seconds), the voltage levels start to rise again by 7.5 to 15 seconds, which suggests that the system has stabilized. Over the course of the disturbance, the frequency decreases from its nominal value of 50 Hz to values of around 47–48 Hz before gradually returning to 50 Hz. Similar to the swing/reference bus, which keeps a fixed angle during simulations, the Egbin bus displays a constant 0.0° angle throughout. This table illustrates how several components (buses) respond in terms of voltage angle, magnitude, and frequency in reaction to an event, capturing the transient behaviour of a power system. It most likely came from a real-time disturbance analysis or dynamic simulation used in grid stability research. At each case a swing bus is being change, a new voltage profile is set up that is quite different from the previous.

CONCLUSSION

The analysis shows that the swing bus's location in the Nigerian 330kV transmission network has a major impact on the network's power flow, voltage profile, line losses, and bus-to-bus distance. The findings demonstrate that the swing bus's ideal location may lower line losses, increase the accuracy and convergence of load flow solutions, and improve the power system's overall stability and dependability. Decisions on power system operation and planning, especially in the Nigerian grid network, might be influenced by the study's conclusions. The approach and findings of the study are applicable to other power systems as well, offering power system engineers. I hereby recommend the following: 1. The ideal swing bus location should be established by taking into account the particular features of the power system. 2. Power system planning: When developing a power system, power system planners should take into account how swing bus location affects the grid network's overall performance. 3. More research: More study is required to examine how swing bus placement affects fault analysis and transient stability, two key facets of power system functioning.

REFERENCES

1) Akisot E. E., Braide S. L., Asuquo E. E, Koledoye T. O., A. J. Onah, Akpama E. J. Analysis And Evaluation of Faults on A 330 Kv Transmission Line Network in Southern Nigeria for Improve Performance, Journal of Emerging Technologies and Innovative Research (JETIR), JETIR January 2022, Volume 9, Issue, 2022
2) Eke, A., Archibong, E., Akisot, E., & Akpama, E. J. (2021). Harmonic Analysis and Evaluation on Nigeria 330kv Lines Network For Effective Energy Planning and Delivery. International Journal of Advances in Engineering and Management (IJAEM), 3(8), 624-629.
3) Inyang Asuquo Akisot E. Akpama E. J, Asuquo Eke, Archibong E. Power Loss Reduction for a Proposed 330 KV Transmission Line for Improve Performance, International Journal of Innovative Science and Research Technology. Volume 6, Issue 7, Pages 1118 – 1124 2021.
4) Ayodele, T. R., Ogunjuyigbe, A. S. O., & Oladele, O. O. Improving the transient stability of Nigerian 330Kv transmission network using static var compensation part I: the base study. Nigerian Journal of Technology, 35(1), 155-166. 2016
5) Ogbuefi, U. C., & Madueme, T. C. A power flow analysis of the Nigerian 330 kV electric power system. 2015
6) Okakwu, I. K., & Ogujor, E. A. Transient stability analysis of the Nigeria 330-kV transmission network. American journal of Electrical power and Energy systems, 6(6), 79-87. 2017.
7) Oluseyi, P. O., Adelaja, T. S., & Akinbulire, T. O. Analysis of the Transient Stability Limit of Nigeria's 330kV Transmission sub-network. Nigerian Journal of Technology, 36(1), 213-226. 2017
8) Currie, G., & Loader, C. Bus network planning for transfers and the network effect in Melbourne, Australia. Transportation Research Record, 2145(1), 8-17.2010
9) Ziaee, O., & Choobineh, F. Optimal location-allocation of TCSCs and transmission switch placement under high penetration of wind power. IEEE Transactions on Power Systems, 32(4), 3006-3014. (2016.
10) Angeles, C. J., Mercader, E. J., Tan, G. E., Pacis, M. C., & Bersano, R. F. December). Fault evaluation and performance of an IEEE Bus 30 power distribution network with distributed generation (DG). In 2017IEEE 9th International Conference on Humanoid, Nanotechnology, Information Technology, Communication and Control, Environment and Management (HNICEM) (pp. 1-6). IEEE. (2017,
11) Li, Y., Feng, B., Li, G., Qi, J., Zhao, D., & Mu, Y. Optimal distributed generation planning in active distribution networks considering integration of energy storage. Applied energy, 210, 1073-1081. 2018
12) Chen, T. H., Chen, M. S., Hwang, K. J., Kotas, P., & Chebli, E. A. Distribution system power flow analysis-a rigid approach. IEEE Transactions on Power Delivery, 6(3), 1146-1152.1991
13) Ake David, EkeAsuquo, Okon Ekpenyong, Gertrude Fischer, Akpama E. Modeling a network with high penetration of hybrid (Solar PV and Wind) renewable energy for Nigeria's future energy sustainability and Economic Development International Journal of Engineering and Science Invention (IJESI)ISSN (Online): 2319-6734, ISSN (Print): 2319-6726www.ijesi.org ||Volume 13 Issue 6 June 2024 || PP 61-67DOI: 10.35629/6734-13066167, Volume 13, Issue 6, PP 61-67, 6/2024
14) Olatomiwa, L., Longe, O. M., Abd'Azeez, T. A., Ambafi, J. G., Jack, K. E., & Sadiq, A. A. Optimal planning and deployment of hybrid renewable energy to rural healthcare facilities in Nigeria. Energies, 16(21), 7259. 2023

License: This is an open access article under the CC BY 4.0 license: https://creativecommons.org/licenses/by/4.0/

Corresponding Author: Asuquo Eke